Journal of Geodynamics 66 (2013) 134–145

Contents lists available at SciVerse ScienceDirect

Journal of Geodynamics

journal homepage: http://www.elsevier.com/locate/jog

Sediment loading at the southern Chilean trench and its tectonic implications

Eduardo Contreras-Reyes[a,*], Jorge Jara[a], Andrei Maksymowicz[a,b], Wilhelm Weinrebe[c]

[a] Departamento de Geofísica, Facultad de Ciencias Físicas y Matemáticas, Universidad de Chile, Santiago, Chile
[b] Departamento de Geología, Facultad de Ciencias Físicas y Matemáticas, Universidad de Chile, Santiago, Chile
[c] GEOMAR – Helmholtz-Centre for Ocean Research, Kiel, Germany

ARTICLE INFO

Article history:
Received 16 December 2012
Received in revised form 21 February 2013
Accepted 24 February 2013
Available online 14 March 2013

Keywords:
Oceanic lithosphere
Sediment loading
Outer rise
Trench
Accretionary prism
Subduction channel
Valdivia fracture zone
Mocha Block

ABSTRACT

Non erosive margins are characterized by heavily sedimented trenches which obscure the morphological expression of the outer rise; a forebulge formed by the bending of the subducting oceanic lithosphere seaward of the trench. Depending on the flexural rigidity (D) of the oceanic lithosphere and the thickness of the trench sedimentary fill, sediment loading can affect the lithospheric downward deflection in the vicinity of the trench and hence the amount of sediment subducted. We used seismic and bathymetric data acquired off south central Chile, from which representative flexural rigidities are estimated and the downward deflection of the oceanic Nazca plate is studied. By flexural modeling we found that efficient sediment subduction preferentially occurs in weak oceanic lithosphere (low D), whereas wide accretionary prisms are usually formed in rigid oceanic lithosphere (high D). In addition, well developed forebulges in strong oceanic plates behaves as barrier to seaward transportation of turbidites, whereas the absence of a forebulge in weak oceanic plates facilitates seaward turbidite transportation for distances >200 km.

1. Introduction

The thermal subsidence model has successfully predicted the increase in seafloor depth as the oceanic lithosphere cools and contracts as it spreads away from the mid ocean ridge axis (Parsons and Sclater, 1977; Stein and Stein, 1992; Gouturbe and Hillier, 2013). Eventually the oceanic lithosphere becomes so dense that it should founder at a subduction zone (e.g., Stern, 2002). This model, however, does not predict the seafloor depth near subduction zones, where the lithosphere bends into the trench, producing a prominent bathymetric bulge, the outer rise and deep trench. The wavelength and amplitude of the outer rise depend on the rheology and stress state of the oceanic plate (e.g., Caldwell et al., 1976; McNutt and Menard, 1982; Levit and Sandwell, 1995).

Non erosive margins are usually characterized by thick trench fill sediment which obscures the morphologic expression of the outer rise in the vicinity of the trench or deformation front. In addition, thick trench fill sediment represents an additional load on the oceanic lithosphere. The local response of the lithosphere upon sediment loading depends on the sediment thickness, flexural rigidity $D = (ET_e^3/12(1-\nu^2))$, and regional stresses. D is a measure of the resistance of the lithosphere to flexure in response to loading. The Young's modulus, E, and Poisson's ratio, ν are material properties commonly treated as constant. Sensitive analysis shows that D is much more sensitive to T_e than E and ν (see discussion of Contreras-Reyes and Osses, 2010). In the case of a weak lithosphere (low D), thick sediment may considerably increase the local flexure of the lithosphere near the trench, affecting the amount of sediment subducted. In order to test this hypothesis, we predict the top of the oceanic lithosphere using a flexural elastic model which is constrained with high resolution seismic reflection and bathymetric data along the southern central Chile margin. We choose this study region because of the existence of a large amount of available geophysical data (e.g., Flueh and Grevemeyer, 2005; Scherwath et al., 2009; Contreras-Reyes et al., 2010; Moscoso et al., 2011) sampling the uppermost part of the oceanic Nazca plate at different thermal ages (Voelker et al., 2011a).

Since sedimentation at the trench varies over time, the flexure in the vicinity of the trench is not a steady-state process but time-dependent. The southern central Chile trench started to be considerably sedimented as a response to a rapid increase of glacial age sediment supply to the trench during the middle Pliocene (Melnick and Echtler, 2006). The high average sedimentation rate since the Pliocene linked to fast denudation of the Andes

* Corresponding author at: Departamento de Geofísica, Facultad de Ciencias Físicas y Matemáticas, Universidad de Chile, Blanco Encalada 2002, Santiago, Chile. Tel.: +56 229784296.
E-mail address: econtreras@dgf.uchile.cl (E. Contreras-Reyes).

0264-3707/$ – see front matter © 2013 Elsevier Ltd. All rights reserved.
http://dx.doi.org/10.1016/j.jog.2013.02.009

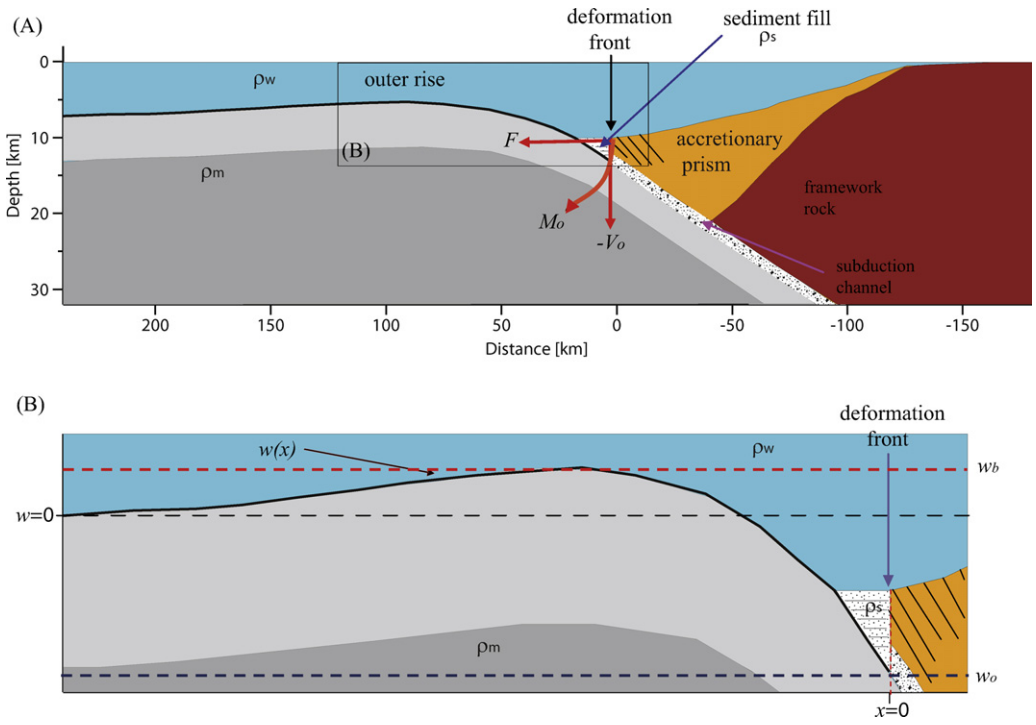

Fig. 1. (A) Bending of the lithosphere at an ocean trench due to the applied vertical shear force V_o, horizontal force F and bending moment M_o. ρ_m, ρ_s and ρ_w are the mantle, trench-sediment and water density, respectively. (B) Schematic representation of topography defining the deflection curve $w(x)$. w_o and w_b are the minimum and maximum flexure, respectively.

Cordillera and that the steady decrease of the subduction rate of the incoming oceanic Nazca plate had shifted the margin from erosive to accretionary during the Pliocene (Melnick and Echtler, 2006). This process has facilitated the formation of a frontal accretionary prism (FAP) ~7–50 km wide (Contreras-Reyes et al., 2010). Seismic data show that both the subduction channel thickness and FAP size largely vary along the southern central Chile margin (e.g., Contreras-Reyes et al., 2010; Geersen et al., 2011). In order to predict qualitatively these differences in terms of lithospheric downdeflection at the trench, we model the lithospheric flexure in the vicinity of the deformation front as a function of the sediment thickness, which in turn varies over time. These results provide insights in how the subduction channel and accretionary prism form. In addition, the predicted temporal evolution of the deflected top of the oceanic lithosphere has direct implications for sediment transportation seaward of the trench.

2. Flexural modeling

The flexure of the oceanic lithosphere at trenches has been modelled by many authors as an elastic plate acted upon by a hydrostatic restoring force $g(\rho_m - \rho_w)w$, where w is the plate flexure, g is average gravity, and ρ_m and ρ_w are mantle and water density, respectively (Fig. 1A) (e.g., Caldwell et al., 1976; Turcotte and Schubert, 1982; Levitt and Sandwell, 1995; Contreras-Reyes and Osses, 2010). If the applied load consists of a bending moment M, the deflection w of the plate is governed by the following ordinary differential equation:

$$-\frac{d^2M}{dx^2} + (\rho_m - \rho_w)wg = q(x) \tag{1}$$

where $q(x)$ is the load acting on the plate and the bending moment and shear force V are related to the negative curvature of the plate $\kappa = (-d^2w/dx^2)$ by the flexural rigidity D by:

$$M = -D\frac{d^2w}{dx^2} \tag{2}$$

and

$$V = \frac{dM}{dx} - F\frac{dw}{dx} \tag{3}$$

In order to include the effect of sediment loading at the trench basin in our flexural model, we incorporate the sediment loading $q(x) = (\rho_s - \rho_w)gh_s(x)$, where ρ_s and $h_s(x)$ are the sediment density and thickness, respectively (Fig. 1B). Thus, we solve (1) using the method of finite differences (Contreras-Reyes and Osses, 2010). It is worth noting that effect of forces and moments acting arcward of the trench are concentrated to the vertical shear force V_o and bending moment M_o at the trench (Turcotte and Schubert, 1982). V_o and M_o cannot be independently measured, and they are modeled jointly with T_e (Contreras-Reyes and Osses, 2010).

Because the sedimented trench fill or trench basin is located seaward of the trench axis (Fig. 1), we modeled explicitly this load in our approach. To show the effect of sediment loading on the downward deflection of the lithosphere, we calculated $w(x)$ for a trench basin with three different sedimentary thickness distributions ($h_s(x)$) which are shown in Fig. 2A. We computed $w(x)$ for an elastic plate with T_e of 10 km, and 35 km and sediment densities of 2100 kg/m^3 and 2700 kg/m^3 (Bray and Karig, 1985). Results are plotted in Fig. 2B–E. Fig. 2B and D shows representative weak oceanic plate with little elastic strength (T_e = 10 km), resulting in a small forebulge (w_b in Fig. 1B). This morphology is typical of hot and young oceanic plate (<25 Ma) observed in the southeastern Gulf of Alaska (Harris and Chapman, 1994) and south Chile (Contreras-Reyes and Osses, 2010). Fig. 2C and E shows representative rigid oceanic plate with greater elastic strength (T_e = 35 km) with a well developed outer rise (high w_b of ~700 m). The effect of episodic trench sedimentation is studied for these two end members models when $h_s(x)$ increase from $h_s^1(x)$ to $h_s^2(x)$, and then successively from $h_s^2(x)$ to $h_s^3(x)$. The amplitude and wavelength of the downdeflection is larger for the weaker plate (Fig. 2B and D). This process allows the seaward accommodation of sediment and locally the

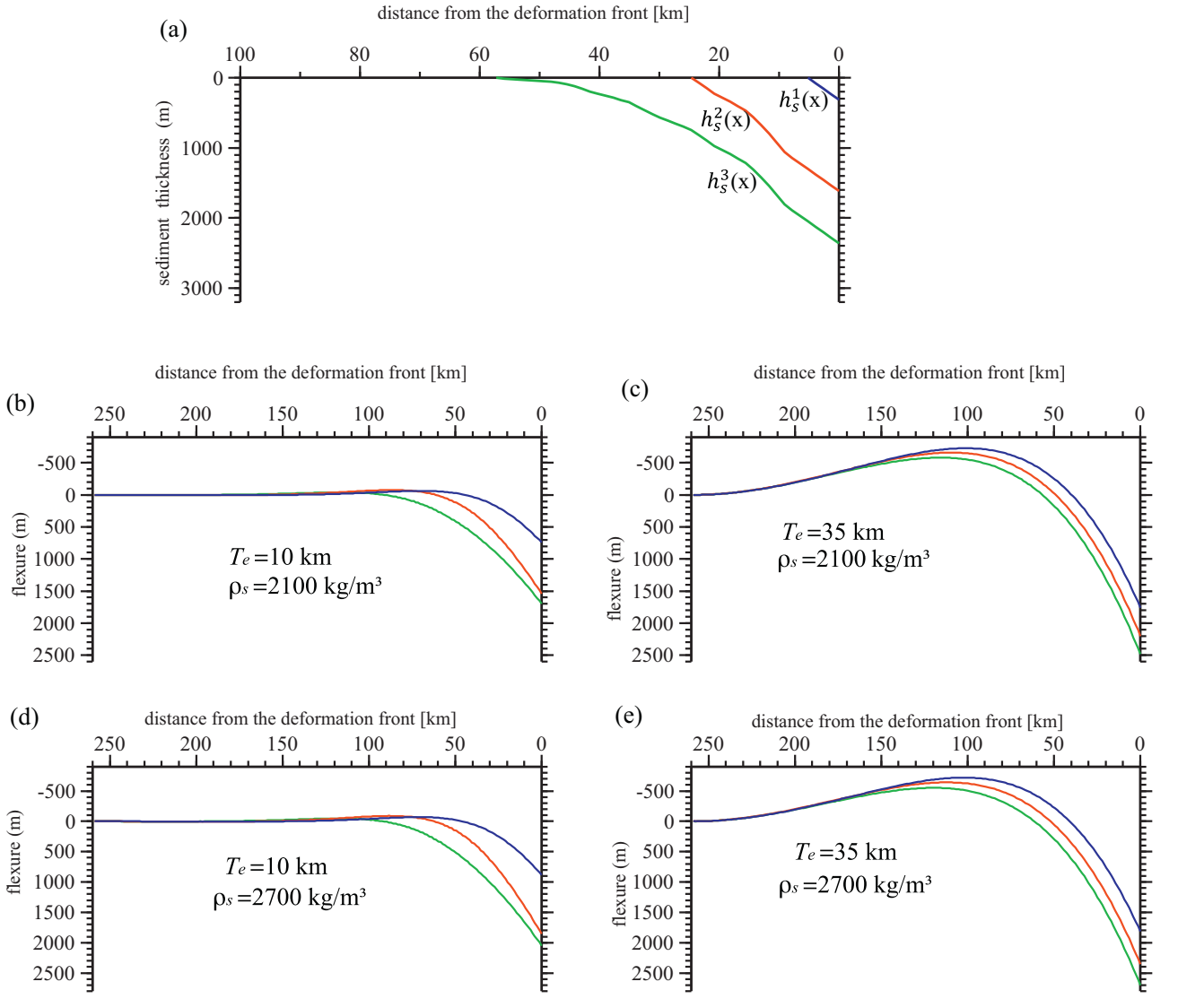

Fig. 2. (A) Trench fill thicknesses $h_s(x)$ which defines a sediment loading $q(x) = (\rho_s - \rho_w)gh_s(x)$ over the lithosphere as shown in Fig. 1B. (B)–(E) Solid curves show the flexure of the lithosphere for an elastic plate for the three sediment thicknesses shown in (A) for different values of T_e and ρ_s. Numeric values used for calculations are shown in Table 1.

downward movement of the oceanic plate beneath the overriding plate.

3. Geodynamic setting off south central Chile

3.1. Plate age and morphology of the outer rise

The southern central Chilean margin is characterized by subduction of the oceanic Nazca plate beneath South America at a current convergence rate of ~6.6 cm/a (Angermann et al., 1999).

Table 1
Values of parameters and constants used in flexural modeling.

Name	Symbol	Value	Unit
Young's modolus	E	70×10^9	Pa
Acceleration due to gravity	g	9.81	$m\,s^{-2}$
Poisson's ratio	ν	0.25	
Mantle density	ρ_m	3300	$kg\,m^{-3}$
Sediment density	ρ_s	2300–2700	$kg\,m^{-3}$
Water density	ρ_w	1030	$kg\,m^{-3}$

This convergence rates remain approximately constant owing to the position of the rotation poles for Nazca-South America (see Appendix A). North of ~34° S, the incoming oceanic Nazca plate was formed at the Pacific-Nazca spreading center (East Pacific Rise) more than 38 Myr ago (Tebbens et al., 1997), whereas between ~34° and 46° S it was created at the Nazca-Antarctic spreading center (Chile Rise) within the past 35 Ma (Herron et al., 1981) (Fig. 3). The age of the oceanic Nazca plate (Tebbens et al., 1997) along the Peru-Chile trench increases from 0 Ma at the Chile Triple Junction (CTJ) with the Antarctic and South American plates (~46.4° S) to ~38 Ma at the subduction of the Juan Fernández Ridge (JFR).

Fracture zones (FZs) cut the Chile Rise into several segments, resulting in abrupt changes of thermal states along the plate boundary (Fig. 3). A striking feature is the Valdivia FZ system composed of ten individual fracture zones (Tebbens et al., 1997) with a total offset of about 600 km (Fig. 3). Another striking oceanic feature is the Mocha Block (MB); which is defined by the triangulation of the Chile Trench, Valdivia FZ system, and the Mocha FZ (Fig. 3). This block separates young and hot oceanic plate in the south from old and cold oceanic lithosphere in the north. The seafloor formed south of the MB is about 500–1000 m shallower than north of it,

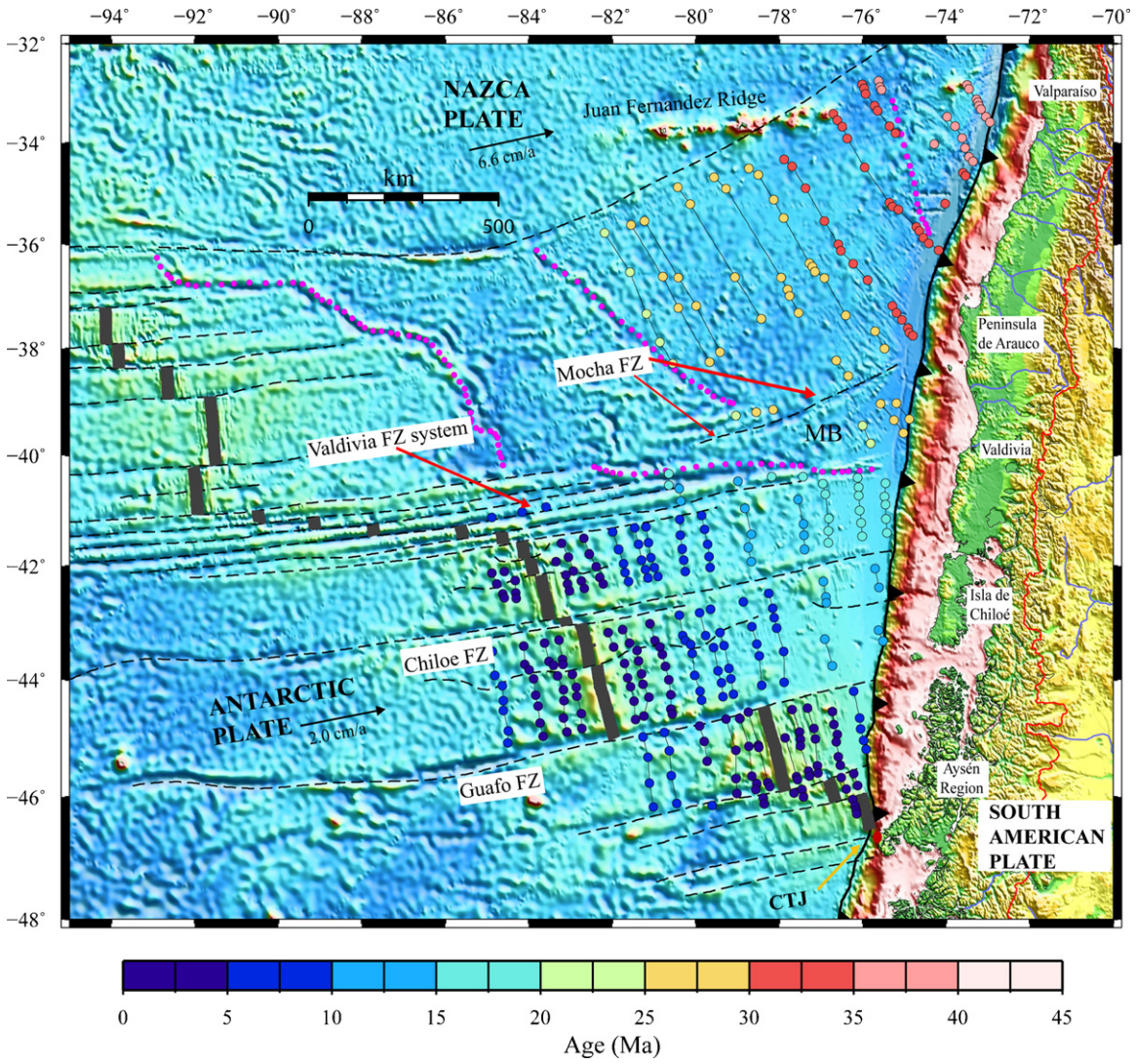

Fig. 3. The age of the incoming Nazca plate is indicated by the colored circles (Tebbens et al., 1997). The projection lines of the fracture zones are given as gray stippled lines. (For interpretation of the references to color in this figure legend, the reader is referred to the web version of the article.)

reflecting the buoyancy of the hot and young oceanic Nazca plate in this region. Hereafter, we refer to the Maule segment as the region south of the JFR and north of the MB, which is a zone characterized by a rigid and cold incoming oceanic lithosphere, and the Chiloé segment as the region south of the MB and north of the CTJ, which is a region characterized by a weak and hot incoming oceanic lithosphere.

The flexural rigidity of the oceanic incoming plate influences the morphology of the outer rise, as is clearly observed in high resolution bathymetric data (Fig. 4). The outer rise along the Maule segment is well developed with an uplifted seafloor 40–50 km seaward of the trench, where well developed bending related faults striking approximately parallel to the trench are observed (Fig. 4A). In contrast, along the Chiloé segment, no pronounced outer rise bulge exists and turbidites propagate further seaward up to 200 km from the deformation front (Fig. 4B). The latter observation is more clearly observed in high resolution seismic reflection data, where old plate located north of the MB (Fig. 5A and B) is characterized by a well developed outer rise bulge, which reflects the large rigidity of the oceanic plate in this segment of the margin. Further south, the oceanic plate is deflected downward without an outer rise bulge allowing the seaward transportation of turbidites (Fig. 5C–E).

3.2. Trench sedimentation

The southern central Chile trench between 34° S and 46° S is heavily sedimented, the result of sediments delivered by the rivers and rapid glaciation denudation of the Andes (Thornburg et al., 1990). Sediment transport from the continent to the trench is controlled by submarine landslides, submarine canyons, and turbidity currents (Voelker et al., 2011b). Within the trench, turbidites migrate to the north as the seafloor depth becomes deeper with the plate age (Fig. 3). The seafloor is only 3.5 km deep in the vicinity of the incoming Chile Rise, where the plate age is 0 Ma. Here, the trench fill is almost devoid of sediments, which is explained by the sediment migration towards the south and north due to the subsidence of the older oceanic lithosphere (Fig. 4). As the oceanic plate becomes older to the north, seafloor depth increases rapidly, reaching a depth of ~4 km at 43° S and ~5.8 km at 33° S. The trench fill thickness between 34° and ~45° S ranges between 1.5 and 3.3 km, while north of the JFR sedimentary thickness is only about 0.4–0.5 km (von Huene et al., 1997). The JFR behaves like a barrier for trench turbidites transport, separating a sediment-starved trench axis to the north from a sediment-flooded axis to the south (von Huene et al., 1997).

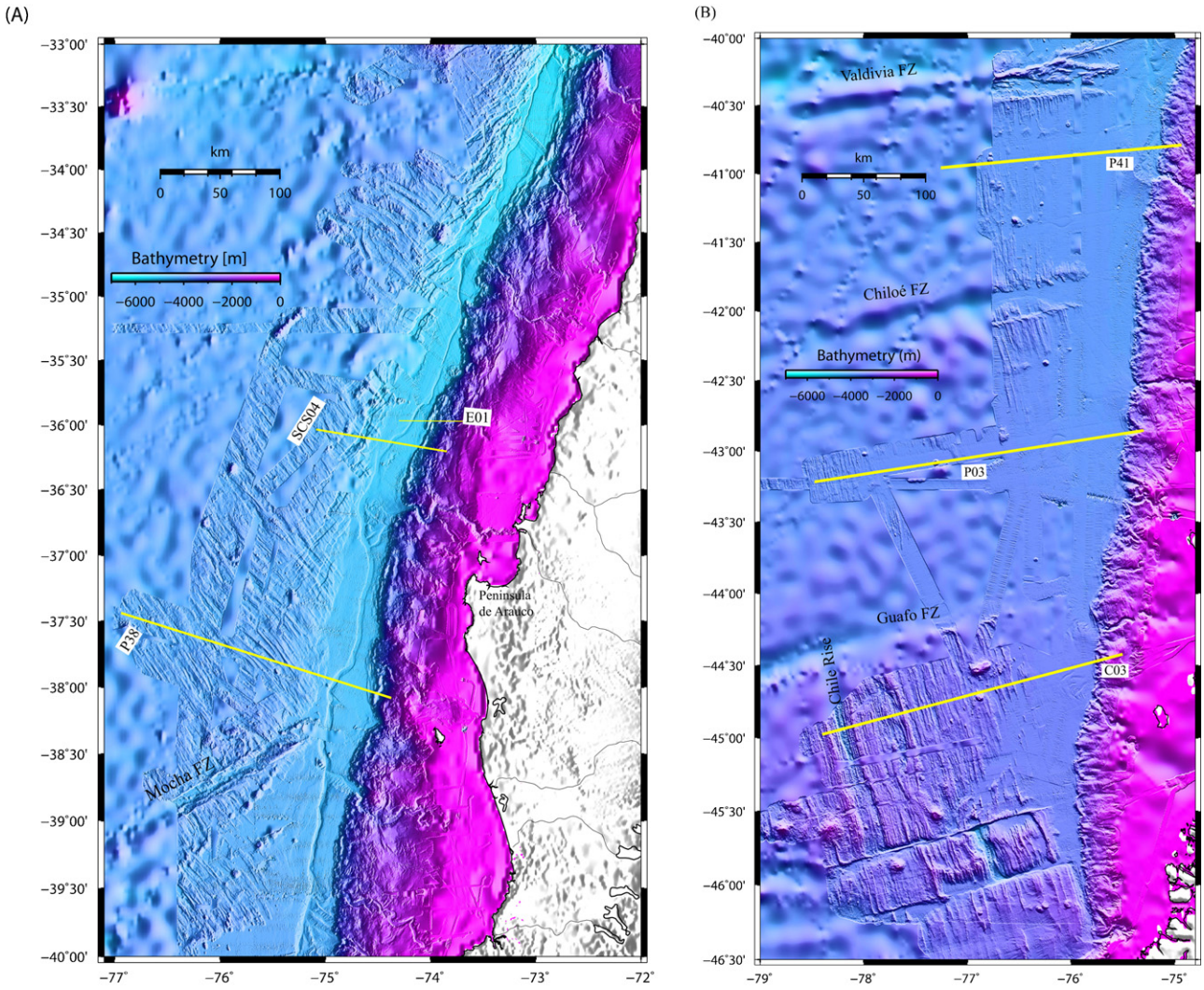

Fig. 4. High resolution bathymetry of south-central Chile. (A) Maule segment and (B) Chiloé segment.

3.3. *The frontal accretionary prism off south central Chile*

The seawardmost part of the south central Chile forearc (33°–46° S) can be characterized by two main segments that present differences in their FAP sizes. The northern Maule segment is characterized by a FAP 20–50 km wide (Contreras-Reyes et al., 2010; Moscoso et al., 2011), while the southern Chiloé segment is characterized by a small FAP (<10 km wide) and efficient sediment subduction (Scherwath et al., 2009). Seismic refraction data provide constraints for this observation (Fig. 6) where the location of the continental framework-FAP contact is well resolved by a steep horizontal velocity gradient. The continental framework-FAP contact defines the size of the frontal accretionary prism. Moscoso et al. (2011) showed a high resolution seismic tomography model off the Maule region (∼35° S) which consistently shows a wedge shaped body with typical sedimentary velocities of 2.5–5.0 km/s indicative of the frontal accretionary prism. At about 50 km landward of the deformation front, there is a major steep horizontal velocity gradient suggesting the landward edge of the FAP (Fig. 6A). In contrast, Scherwath et al. (2009) showed the 2D velocity off Aysén with a rather narrow frontal accretionary prism 5–7 km wide (Fig. 6B), which is limited landward by a sharp horizontal velocity gradient suggesting a change in rock type.

It is worthnoting that we do not define the FAP size using a specific velocity range, but a steep horizontal velocity gradient at the landward edge of the FAP. Due to sediment compaction, large accretionary prisms comprise faster velocities at their landward edges than small ones. Abrupt horizontal velocity gradients defining the continental framework-FAP contact has been also reported in the Cascadia subduction zone (Trehu et al., 1994; Gerdom et al., 2000) and the southern Ryukyu margin (Klingelhoefer et al., 2012).

An indirect observation for efficient sediment subduction is the small FAP size found in thick sedimented trenches with angle refraction data (Scherwath et al., 2009), which not necessarily correlates with thick subduction channels near the deformation front observed in seismic reflection data (e.g., Diaz-Naveas, 1999; Geersen et al., 2011; Trehu et al., 2012). This apparent inconsistency is due to the usual shallow penetration of MCS data, which images the subduction channel typically in the first 5–10 km of the shallow subduction interface. At these depths, there is a lot of variations in subduction channel thickness both along dip and strike. Thus, thick subduction channel near the deformation front is not a well indicator for efficient sediment subduction in a long term scale. In fact, sediment can be futher down underplated at the base of the accretionary prism when the friction at the subduction interface is high (Contardo et al., 2008; Maksymowicz, revised). Thus, seismic velocities and pronounced velocity gradients provide an indirect but a better clue for sediment subduction in a long term scale.

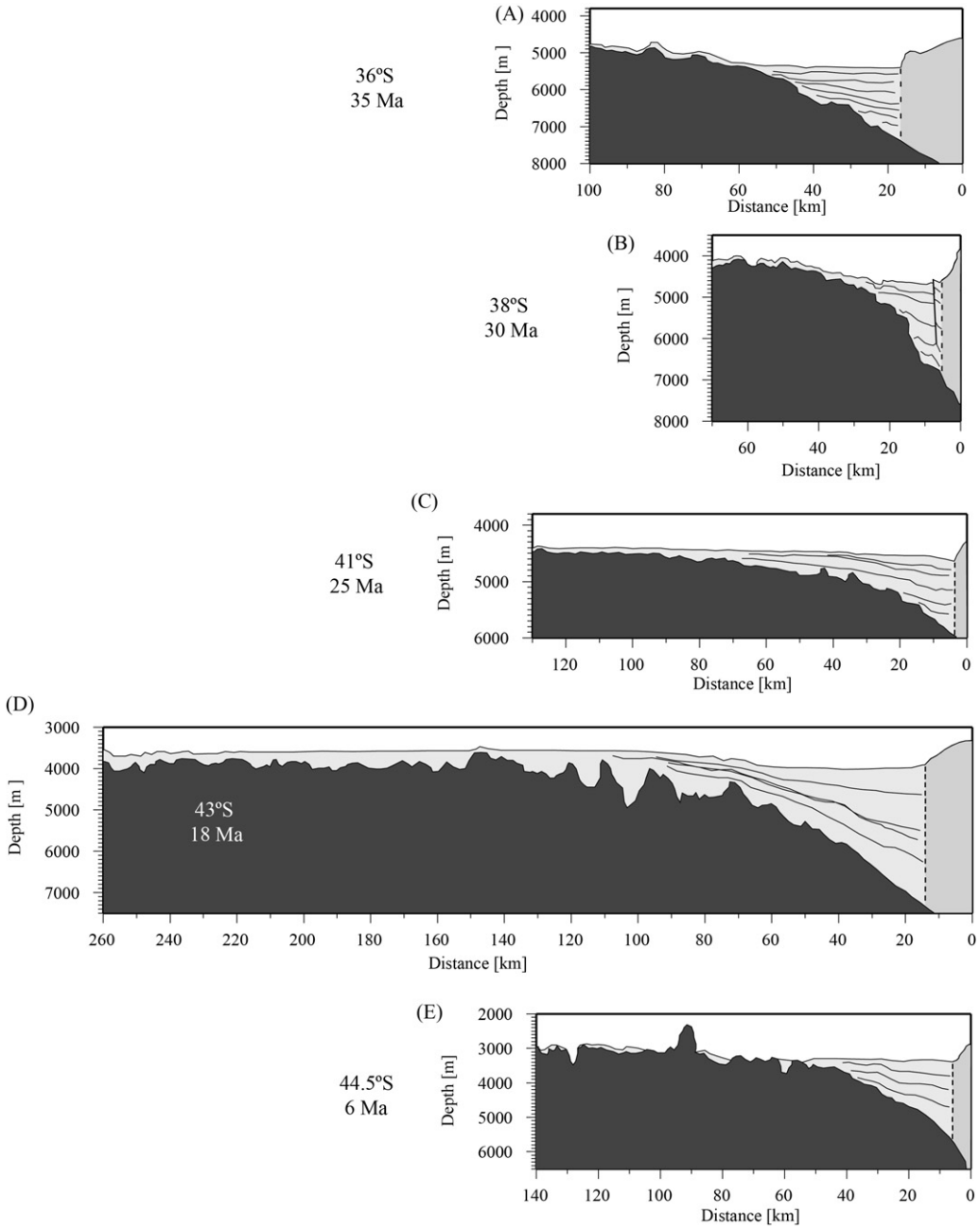

Fig. 5. Interpretative line drawings of seismic reflection lines showing differences in outer rise morphology (Flueh and Grevemeyer, 2005). Light grey shaded areas are accreted sediments while dark grey shaded areas denote oceanic crust (see supplementary material for further seismic details). The dotted line represents the location of the deformation front. For comparison all plots are at the same scale and the oceanic plate age at the deformation front is shown.

3.4. The continental slope off south central Chile

Fig. 7 shows the location of the deformation front and slope shelf break off south central Chile, and hence the wide of the continental slope is inferred. The shelf break is the transition from the continental slope to the continental shelf that occurs landward of most accretionary wedges. Byrne et al. (1988) argued that that change is caused by a large landward increase in the strength of the material within the overriding plate (the backstop). Laboratory modeling experiments indicate that a backstop with a trenchward-dipping upper surface results in the development of a passive forearc basin which overlies the framework rock or continental basement (e.g., Byrne et al., 1988). However, the shelf break should not be necessarily located at the landward edge of the accretionary prism. In fact, seismic observations show that the landward edge of the FAP is located beneath the lower continental slope (seaward of shelf break). This is the case for the FAP between ~43° S and ~45° S (Scherwath et al., 2009; Contreras-Reyes et al., 2010). Nevertheless, the wide of the continental slope represents the possible maximum wide of the accretionary prism. For example, off Maule (Fig. 6A) and off southern Peninsula de Arauco (38° S) (Contreras-Reyes et al., 2010), the landward edge of the FAP is coincident with the location of the shelf break. In contrast, off Aysén (Fig. 6B) and off Isla de Chiloé (Contreras-Reyes et al., 2010), the landward termination of the accretionary prism is located seaward of the shelf break and closer to the trench. Thus, seismic data are necessary to determine more precisely the wide of the accretionary prism. Nevertheless, the continental slope wide is an upper bound for the FAP wide, and a narrow continental slope is an indicator of a small FAP.

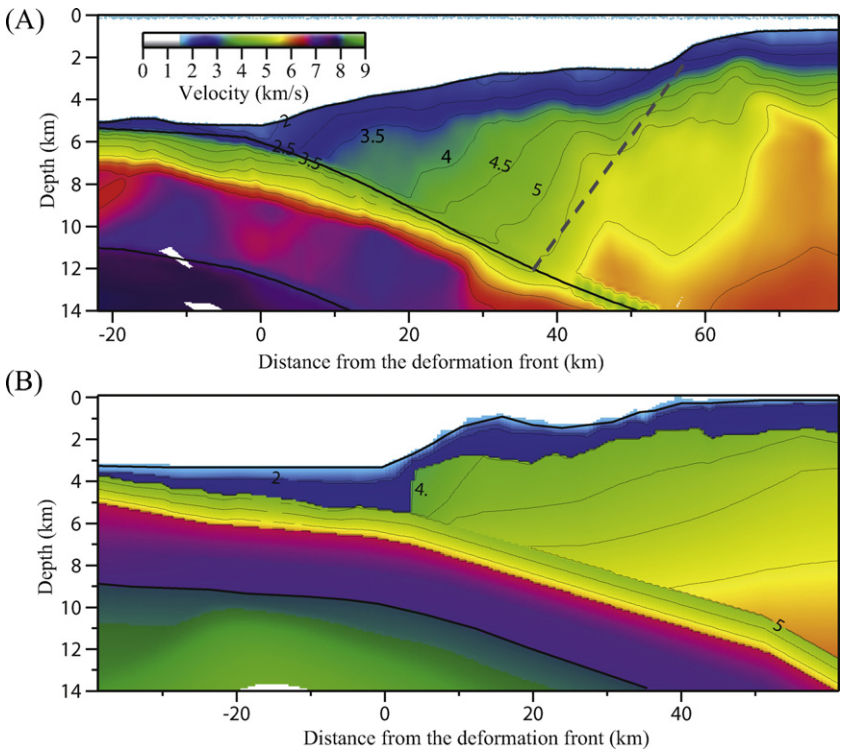

Fig. 6. (A) 2D velocity model off Constitución (∼34.5° S) (Moscoso et al., 2011) representative of the Maule segment. (B) 2D velocity model off Aysén (∼44.5° S) (Scherwath et al., 2009) representative of the Chiloé segment. Note that the landward limit of the FAP is limited by an abrupt horizontal velocity gradient. For the Maule case, the FAP is 40–50 km wide and is coincident by 1–2 km scarp at the shelf break. In contrast, the FAP off Aysén is only ∼7 km wide, and it is coincident with the low-middle slope transition.

Fig. 7 shows that the continental slope is 60–100 km wide between 34° S and 41° S. This segment hosts the Maule segment, the Mocha Block and the northernmost part of the Chiloé segment. South of ∼41° S, the continental slope becomes narrower being only ∼20 km wide in the area of the Chile Triple Junction at ∼46° S. The CTJ region is affected by tectonic erosion enhanced by the Chile Rise subduction, and it is characterized by the absence of an accretionary prism (Scherwath et al., 2009). The narrowing of the continental slope south of ∼41° S is consistent with the small size of the FAP observed by seismic data in most of the area of the Chiloé segment, which is a region characterized by effective sediment subduction (Contreras-Reyes et al., 2010). The area of the Mocha Block (38°–41° S) is more difficult to interpret due to active mass wasting processes of the continental shelf (Geersen et al., 2011) which are perhaps controlled by the complex subduction of the Mocha FZ and Valdivia FZ system. Therefore, more wide-angle seismic data are needed in this zone to map more precisely the size of the FAP.

4. Flexural rigidity of the oceanic Nazca plate

Figs. 4 and 5 show clear differences in the style of deformation of the oceanic lithosphere as at bends into the trench. Along the Maule segment, the plate is rigid and presents a well developed outer rise bulge. This contrasts with the Chiloé segment, where the weak oceanic plate is deflected downward lacking a prominent outer rise bulge, suggesting a contrast in the flexural rigidities between these two segments. In order to estimate this difference, we model the flexure of the oceanic lithosphere along seismic line SCS04 (Fig. 5A) and corridor C03 (Fig. 5E) which are representative of strong and weak oceanic Nazca plate, respectively. The top of the oceanic crust from each line is extracted and plotted in Fig. 8. The curves are compared based on their minimum flexure at the trench axis, in order to compare their maximum flexure peaks. The plot clearly shows the well developed outer rise along the Maule segment (SCS04) which is uplifted by more than 500 m about the undeflected limit. The best fitted elastic thicknesses values are 28 and 15 km for profiles E01 and C03, respectively (see Fig. 8). Hence, the flexural rigidity is about seven times higher along profile E01 than along profile C03.

5. Discussion

5.1. Formation of the subduction channel and frontal accretionary prism

As we demonstrated above, high resolution bathymetric and seismic data indicate the presence of two major tectonic segments with different flexural rigidities along the south central Chile margin. In particular, sediment accretion is more effective in the Maule segment, where the incoming oceanic lithosphere is older (30–38 Ma), rigid and cold. In contrast, efficient sediment subduction occurs where the young (25–5 Ma), hot and weak oceanic Nazca plate subducts beneath South America along the Chiloé segment. In the following, we present a schematic model for the formation of the subduction channel and frontal accretionary prism for a rigid and weak oceanic plates representative of the Maule and Chiloé segments, respectively.

5.1.1. Case of a rigid oceanic plate

Sediment arrives mainly at the trench transported by the incoming oceanic plate and deposition from turbidity currents from the overriding continental plate. As it approaches the inlet of the subduction channel, it undergoes strong longitudinal compression

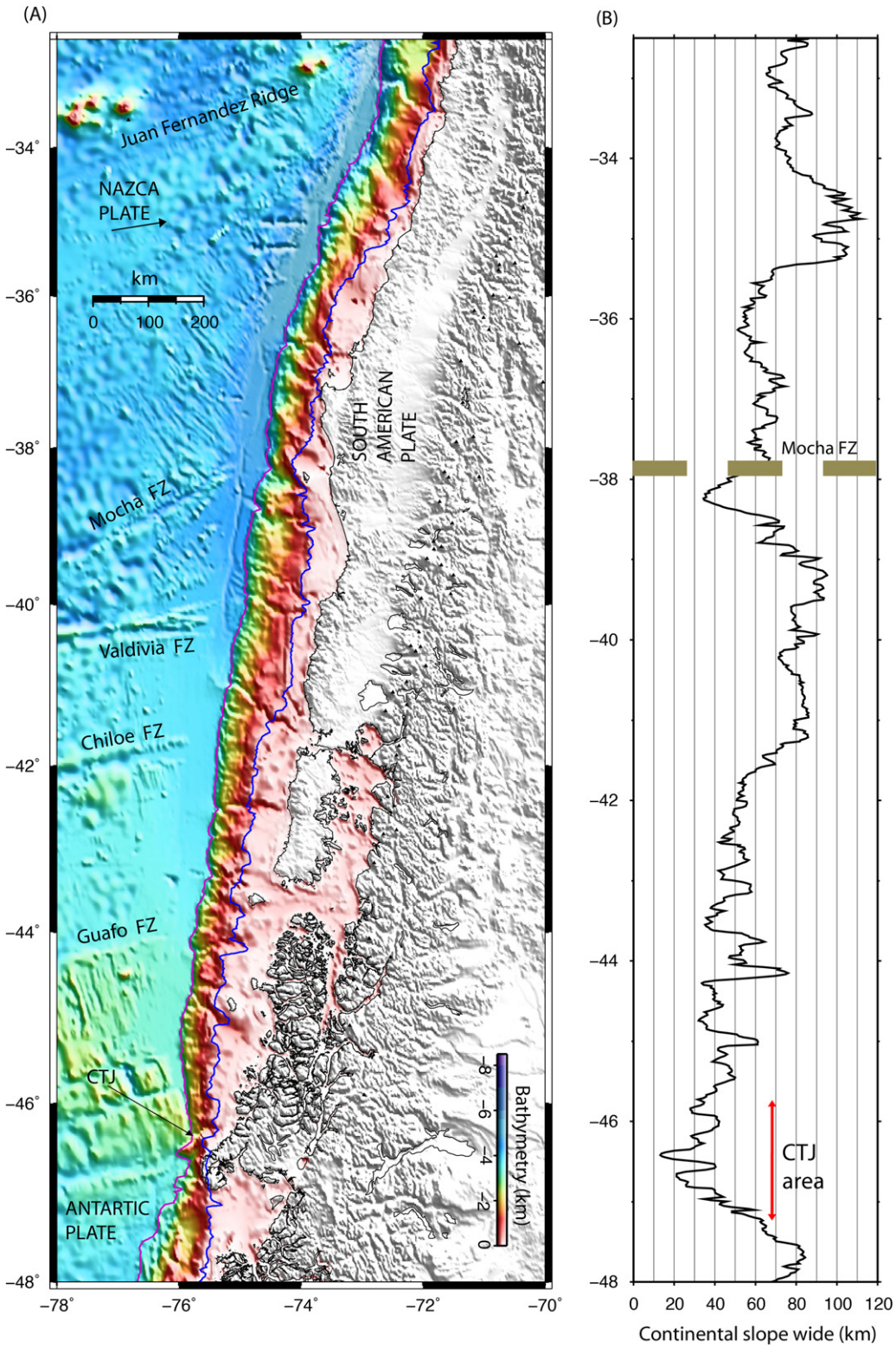

Fig. 7. (A) High resolution bathymetry of south-central Chile. Blue and purple curves denote the location of the shelf break and deformation front, respectively. (B) Wide of the continental slope that is the distance between the deformation front and shelf break. (For interpretation of the references to color in this figure legend, the reader is referred to the web version of the article.)

defining the onset of the deformation front (e.g., Shreve and Cloos, 1986). The rigid incoming oceanic lithosphere presents a well-developed forebulge, which behaves as barrier for seaward sediment transport. Thus, deposited turbidites are confined between the deformation front and trenchward of the outer rise (Fig. 9A).

Sediment deposited in the trench basin would represent a considerable local loading onto the oceanic lithosphere, but the downward deflection is not pronounced and it has a short wavelength due to the high rigidity of the oceanic lithosphere (Fig. 9B). Thus, the limited space for sediment deposition onto the proto subduction channel results in the formation of a thin subduction

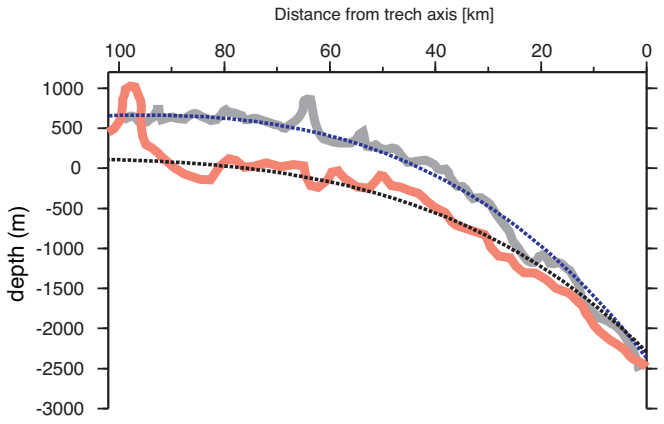

Fig. 8. Flexural modelling along E01 with T_e = 28 km and along C03 with T_e = 15 km (see Table 1 for numeric values used).

channel, whereas the rest of sediment is frontally and/or basally accreted. Since most of the sediments are accreted to the toe of the continent, a wide frontal accretionary prism can be formed. Growth of the frontal prism involves a seaward migration of the deformation front. This model is consistent with the Maule segment, where rigid and cold oceanic lithosphere has facilitated the formation of a relative wide accretionary prism and thin subduction channel (Fig. 9C).

5.1.2. Case of a weak oceanic plate

Similarly, sediment arrives mainly at the trench transported by the incoming oceanic plate and deposition from turbidity currents from the overriding continental plate. The weak incoming oceanic lithosphere does not present a forebulge (Fig. 10A), and seaward sediment transport is possible. Depending on kinematic and dynamic conditions, turbidites reaching the trench can travel seaward several tens of kilometers. Fig. 5C and D shows examples of this case.

Sediment thickness is usually maximum near the deformation front, and it represents a considerable local loading onto the oceanic lithosphere. A pronounced and long wavelength deflection of the lithosphere (Fig. 10B) facilitate the subduction of a large amount of sediments (Fig. 10C). Since most of the sediments subduct, this type of margin presents a thick subduction channel, and few sediments are frontally and/or basally accreted. This model is consistent with the Chiloé segment where weak and hot oceanic lithosphere has facilitated the formation of a relative thick subduction channel and small frontal accretionary prism.

5.2. Tectonic control of flexural rigidity and topographic features of the subducting oceanic lithosphere on the south central Chilean marine forearc

For oceanic lithosphere, the most pronounced changes occur in the first ~20 Myr, when the strongest change in thermal state are observed (e.g., Stein and Stein, 1992). In terms of buoyancy and seafloor morphology, the young incoming Nazca plate along the Chiloé segment presents clear differences compared to the Maule segment (Fig. 4). Particularly, the forebulge is by far more developed in old ocanic plate along the Maule segment while along the Chiloé segment is absent.

The downward deflection as response of sediment loading at the trench plays a crucial role in determining the inlet capacity and hence the amount of subducted or accreted sediment (e.g., Jarrard, 1986; Shreve and Cloos, 1986). Weak and hot oceanic plate presents more pronounced downdeflection at the trench basin due to sediment loading than older oceanic plate (Fig. 7), and therefore weak oceanic plate involves a larger space for sediment subduction (Contreras-Reyes and Osses, 2010). As we have shown above, a larger and wider downdeflection of the oceanic plate is found along the Chiloé segment than along the Maule segment. Consequently, thick and thin subduction channels are developed along the Chiloé and Maule segments, respectively. Seismic data corroborate this observation (Bangs and Cande, 1997; Scherwath et al., 2009; Contreras-Reyes et al., 2010; Geersen et al., 2011; Moscoso et al., 2011).

In terms of a long spatial wavelength scale (λ> 100 km), the Maule segment hosts a rigid oceanic lithosphere compared to the

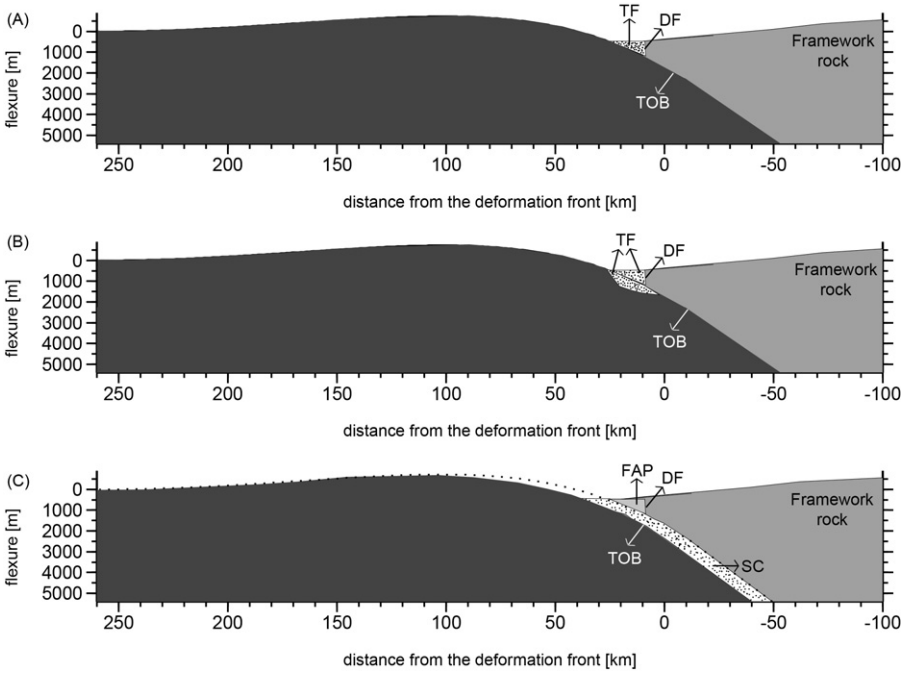

Fig. 9. Cartoon showing the frontal accretionary prism and subduction channel formation for a rigid oceanic lithosphere (i.e., oceanic Nazca plate along the Maule segment).

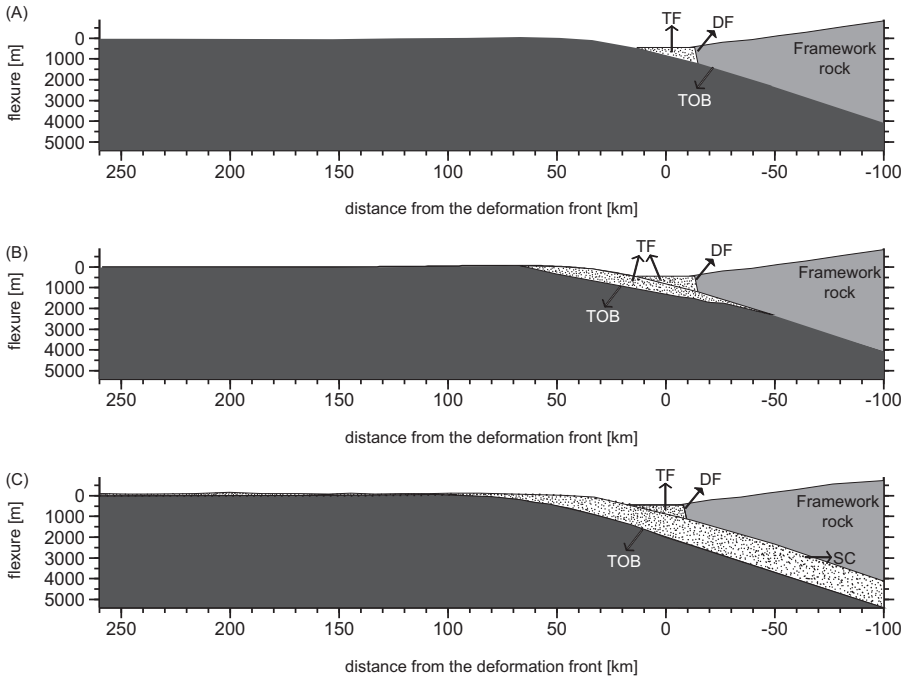

Fig. 10. Cartoon showing the frontal accretionary prism and subduction channel formation for a weak oceanic lithosphere (i.e., oceanic Nazca plate along the Chiloé segment).

weak oceanic plate south of the MB (along the Chiloé segment). Thus, old oceanic Nazca plate (30–38 Ma) is coincident with rigid oceanic lithosphere along the Maule segment, and young oceanic Nazca plate (0–20 Ma) is coincident with weak oceanic lithosphere along the Chiloé segment. However, a consistent and strict reduction in T_e as a function of plate age southward is not expected due to local ($\lambda < 10$ km) anomalies in T_e (Contreras-Reyes and Osses, 2010). Therefore, a consistent and strict increase of subduction channel thickness with the reduction in plate age southward is not expected either as was discussed by Geersen et al. (2011). Rather, we suggest that thick subduction channels are more likely to form where oceanic lithosphere is weak (i.e., low D) and pronounced downward deflection occurs at the trench basin facilitating sediment subduction. Additionally, an increase in the subduction channel thickness is expected in regions where canyon exits increase locally and anomalously the sedimentary thickness and loading at the trench.

The regional nature of flexure of the oceanic lithosphere along the Maule segment is clearly different from the Chiloé segment (Fig. 7), and the regional thermal state of these segments is clearly manifested in the rheological properties of the oceanic Nazca plate. Most likely, these differences are also manifested in the structure of the marine forearc, where the Maule segment host a wide frontal accretionary prism (20–50 km wide) and a thin subduction

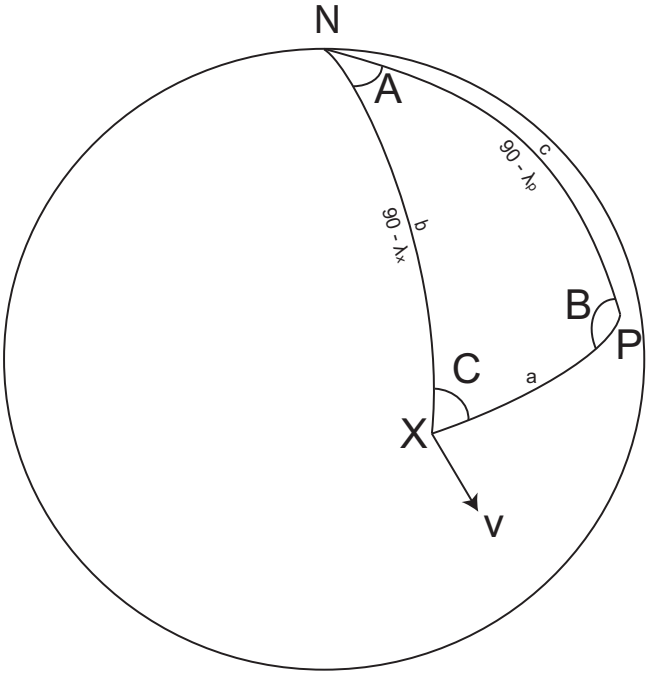

Fig. 11. P: rotation pole, X: point on the plate boundary, and N: North pole. The angular lengths b and c.

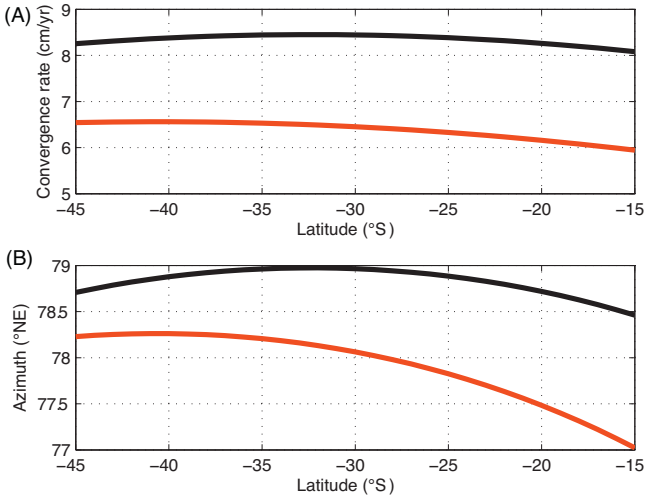

Fig. 12. Convergence rate: (above) black and red curves are the convergence rate between between Nazca and South American plates along strike using the values of DeMets et al. (1990) and Angermann et al. (1999), respectively. (bottom) Black and red curves are the azimuth of the convergence velocity **v** between between Nazca and South American plates along strike using the values of DeMets et al. (1990) and Angermann et al. (1999), respectively. (For interpretation of the references to color in this figure legend, the reader is referred to the web version of the article.)

Table 2
Values of ϕ_p, λ_p and ω for the convergence rate between Nazca and South American plates.

Plates	Rotation pole location (ϕ_p, λ_p)	angular velocity (ω)	References
Nazca-South American	(94° W, 56° N)	7.6×10^{-7} rad/year	DeMets et al. (1990)
Nazca-South American	(91.7° W, 48° N)	5.9×10^{-7} rad/year	Angermann et al. (1999)

channel (<0.5 km thick) compared to the Chiloé segment, which hosts a small FAP (<10 km wide) and a thick subduction channel (1.0–1.5 km thick) (Scherwath et al., 2009; Contreras-Reyes et al., 2010).

6. Summary

The southern central Chile margin (33°–45° S) can be characterized by two main segments that present differences in their frontal accretionary prism size, subduction channel thickness and wide of the continental slope. The northern segment (Maule segment) confined between the Juan Fernández Ridge and the Mocha Block is characterized by a relatively wide FAP 20–50 km wide and a subduction channel typically thinner than 1 km in average. The southern segment (Chiloé segment) is situated between the Mocha Block and the Chile triple junction and is characterized by an extremely small FAP (<10 km wide) and a thick subduction channel (∼1.5 km).

These two segments are marked by the thermal and rheological properties of the subducting oceanic Nazca plate. The oceanic lithosphere is old (30–38 Ma), cold and rigid along the Maule segment, whereas along the Chiloé segment, the subducting plate is young (0–25 Ma), hot and weak. These differences are manifested in the elastical properties of the oceanic lithosphere and the morphology of the outer rise. In fact, the forebulge is well developed along the Maule segment, whereas along the Chiloé segment the outer rise is practically absent. These differences in the mechanical behavior of the oceanic lithosphere are also manifested in the amplitude and wavelength of the lithospheric downdeflection at the trench fill. The weak oceanic plate along the Chiloé segment presents a pronounced downdeflection beneath the heavy sediment trench, whereas the stronger and cold oceanic lithosphere along the Maule segment downdeflects relatively little.

Bathymetric and seismic data reveal that the well developed forebulge along the Maule segment behaves as barrier for westward sediment transport, confining a trench fill of ∼40 km wide in average. In contrast, the absence of a forebulge along the Chiloé segment had facilitated the westward sediment migration reaching distances of up to 240 km from the deformation front. The Mocha Block is a remarkable oceanic topographic feature, and it defines the transition zone from the Maule to the Chiloé segments.

Acknowledgements

Eduardo Contreras-Reyes acknowledges the support of the Chilean National Science Foundation (FONDECYT) project 11090009. We thank Andrés Folguera, and the Editor Randell Stephenson for their constructive reviews of the original manuscript. Fruitful discussions with Anne Trehu are greatly appreciated.

Appendix A. Convergence rate between Nazca and South American plates

Given the rotation pole location (ϕ_p, λ_p) and angular velocity (ω) for the displacement between plate A and B, the velocity of convergence V can be calculated trough Fowler (1990):

$$V = \omega R \sin a \tag{4}$$

where R is the radius of the Earth and a is the angle length shown in Fig. 11:

The angle length a can be calculated via Fowler (1990):

$$\cos(a) = \cos\left(\frac{\pi}{2} - \lambda_x\right)\cos\left(\frac{\pi}{2} - \lambda_p\right) + \sin\left(\frac{\pi}{2} - \lambda_x\right)\sin\left(\frac{\pi}{2} - \lambda_p\right) + \cos(\phi_p - \phi_x) \tag{5}$$

or

$$a = cos^{-1}[sin\lambda_x sin\lambda_p + cos\lambda_x cos\lambda_p)cos(\phi_p - \phi_x)] \tag{6}$$

where ϕ_x and λ_x correspond to the study point.

On the other hand, the azimuth of convergence β can be calculated as $\beta = \pi/2 + c$, where c can be found using:

$$c = sin^{-1}\left(\frac{cos\lambda_p sin(\phi_p - \phi_x)}{sin\, a}\right) \tag{7}$$

Fig. 12 shows the results using the values of Table 2.

Appendix B. Supplementary data

Supplementary data associated with this article can be found, in the online version, at doi:http://dx.doi.org/10.1016/j.jog.2013.02.009.

References

Angermann, D., Klotz, J., Reigber, C., 1999. Space-geodetic estimation of the Nazca-South America Euler vector. Earth and Planetary Science Letters 3 (171), 329–334.
Bangs, N.L., Cande, S.C., 1997. Episodic development of a convergent margin inferred from structures and processes along the southern Chile margin. Tectonics 16 (3), 489–503.
Bray, C.J., Karig, D.E., 1985. Porosity of sediments in accretionary prisms and some implications for dewatering processes. Journal of Geophysical Research 90 (B1), 768–778.
Byrne, D.E., Davis, D.M., Sykes, L.R., 1988. Loci and maximum size of thrust earthquakes and the mechanics of the shallow region of subduction zones. Tectonics 7 (4), 833–857.
Caldwell, J.G., Haxby, W.F., Karig, D.E., Turcotte, D.L., 1976. On the applicability of a universal elastic trench profile. Earth and Planetary Science Letters 31, 239–246.
Contardo, X., Cembrano, J., Jensen, A., Díaz-Naveas, J., 2008. Tectono?sedimentary evolution of marine slope basins in the Chilean forearc (33°30′–36°50′ S): insights into their link with the subduction process. Tectonophysics 459 (1–4), 206–218.
Contreras-Reyes, E., Osses, A., 2010. Lithospheric flexure modeling seaward of the Chile trench: implications for oceanic plate weakening in the Trench Outer Rise region. Geophysical Journal International 182 (1), 97–112, http://dx.doi.org/10.1111/j.1365-246X.2010.04629.x.
Contreras-Reyes, E., Flueh, E.R., Grevemeyer, I., 2010. Tectonic control on sediment accretion and subduction off south-central Chile: implications for coseismic rupture processes of the 1960 and 2010 megathrust earthquakes. Tectonics, http://dx.doi.org/10.1029/2010TC002734.
DeMets, C., Gordon, R., Argus, D., Stein, S., 1990. Current plate motions. Geophysical Journal International 101, 425–478.
Diaz-Naveas, J.L., 1999. Sediment subduction and accretion at the Chilean convergent margin between 35° and 40° S, Ph.D. Thesis, Ch.-A.-Universitaet, Kiel, Germany.
Flueh, E.R., Grevemeyer, I. (Eds.), 2005. TIPTEQ SONNE Cruise SO-181, from the Incoming Plate to mega Thrust EarthQuakes, Geomar Rep. 102, Geomar, Kiel, Germany.
Fowler, C.M.R., 1990. The Solid Earth, an introduction to Global Geophysics. Cambridge University Press, Cambridge, UK.
Geersen, J., Behrmann, J.H., Voelker, D., Krastel, S., Ranero, C.R., Diaz-Naveas, J., Weinrebe, W., 2011. Active tectonics of the South Chilean marine fore arc (35° S–40° S). Tectonics 30, TC3006, http://dx.doi.org/10.1029/2010TC002777.
Gerdom, M., Trehu, A.M., Flueh, E.R., Klaeschen, D., 2000. The continental margin off Oregon from seismic investigations. Tectonophysics 329, 79–97.

Gouturbe, B., Hillier, J.K., 2013. An integation to optimally constrain the thermal structure of the oceanic lithosphere. Journal of Geophysical Research 118, http://dx.doi.org/10.1029/2012JB009527.
Harris, R., Chapman, D., 1994. A comparison of mechanical thickness estimates from trough and seamount loading in the southeastern Gulf of Alaska. Journal of Geophysical Research 99 (B5), 9297–9317.
Herron, E.M., Cande, S.C., Hall, B.R., 1981. An active spreading centre collides with a subduction zone, a geophysical survey of the Chile margin triple junction. Geological Society of America Memoirs 154, 683–701.
Jarrard, R.D., 1986. Relations among subduction parameters. Reviews of Geophysics 24 (2), 217–284.
Klingelhoefer, F., Berthetb, T., Lallemand, S., Schnurle, P., Lee, C.-S., Liu, C.-S., McIntosh, K., Theunissen, T., 2012. P-wave velocity structure of the southern Ryukyu margin east of Taiwan: results from the ACTS wide-angle seismic experiment. Tectonophysics 578, 50–62, http://dx.doi.org/10.1016/j.tecto.2011.10.010.
Levitt, D.A., Sandwell, D.T., 1995. Lithospheric bending at subduction zones based on depth soundings and satellite gravity. Journal of Geophysical Research 100, 379–400.
Maksymowicz, A. Dynamic mass balance of rebuilding an accretionary prism after tectonic erosion related to spreading ridge subduction: Golfo de Penas (south of the Chile triple junction), Geo-Marine Letters, revised.
McNutt, M.K., Menard, H.W., 1982. Constraints on yield strength in the oceanic lithosphere derived from observations of flexure. Geophysical Journal of the Royal Astronomical Society 71, 363–394.
Melnick, D., Echtler, H., 2006. Inversion of forearc basins in south-central Chile caused by rapid glacial age trench fill. Geology 34 (9), 709–712.
Moscoso, E., Grevemeyer, I., Contreras-Reyes, E., Flueh, E.R., Dzierma, Y., Rabbel, W., Thorwart, M., 2011. Revealing the deep structure and rupture plane of the 2010 Maule, Chile Earthquake (Mw = 8.8) using wide angle seismic data. Earth and Planetary Science Letters 307 (1-2), 147–155, http://dx.doi.org/10.1016/j.epsl.2011.04.025.
Parsons, B., Sclater, J.G., 1977. An analysis of the variation of oceanic floor bathymetry and heat flow with age. Journal of Geophysical Research 82, 803–827.
Scherwath, M., Contreras-Reyes, E., Flueh, E.R., Grevemeyer, I., Krabbenhoeft, A., Papenberg, C., Petersen, C.J., Weinrebe, R.W., 2009. Deep lithospheric structures along the southern central Chile margin from wide-angle P-wave modelling. Geophysical Journal International 179 (1), 579–600.
Shreve, R., Cloos, M., 1986. Dynamics of sediment subduction, melange formation, and prism accretion. Journal of Geophysical Research 91 (B10), http://dx.doi.org/10.1029/0JGREA000091000B10010229000001, issn: 0148-0227.
Stein, C.A., Stein, S., 1992. A model for the global variation in oceanic depth and heat-flow with lithospheric age. Nature 359, 123–129.
Stern, R.J., 2002. Subduction zones. Reviews of Geophysics 40 (4), 1012, http://dx.doi.org/10.1029/2001RG000108.
Tebbens, S.F., Cande, S.C., Kovacs, L., Parra, J.C., LaBrecque, J.L., Vergara, H., 1997. The Chile ridge: a tectonic framework. Journal of Geophysical Research 102 (B6), 12035–12060, http://dx.doi.org/10.1029/96JB02581.
Thornburg, T.M., Kulm, D.M., Hussong, D.M., 1990. Submarine-fan development in the southern Chile trench: a dynamic interplay of tectonics and sedimentation. Geological Society of America Bulletin 102, 1658–1680.
Trehu, A.M., Asudeh, I., Brocher, T.M., Luetgert, J.H., Mooney, W.D., Nabelek, J.L., Nakamura, Y., 1994. Crustal arquitecture of the Cascadia forearc. Science 266, 237–243.
Trehu, A., Tryon, M., Contreras-Reyes, E.V., the shipboard party of the 2012 Chile, 2012. Structure and deformation of the accretionary prism up-dig from the patch of greatest slip during the 2010 Maule earthquake. In: Conferencia Cooperación Chile-Estados Unidos en Oceanografía, 8–10 August, Universidad de Concepción WORKSHOP, Chile.
Turcotte, D., Schubert, G., 1982. Geodynamics-Applications of Continuum Physics to Geological Problems. John Wiley, Hoboken, NJ.
Voelker, D., Grevemeyer, I., Stipp, M., Wang, K., He, J., 2011a. Thermal control of the seismogenic zone of southern central Chile. Journal of Geophysical Research 116, B10305, doi:10.1029/2011JB008247.
Voelker, D., Scholz, F., Geersen, J., 2011b. Analysis of submarine landsliding in the rupture area of the 27 February 2010 Maule earthquake, Central Chile. Marine Geology 288, 79–89, http://dx.doi.org/10.1016/j.margeo.2011.08.003.
von Huene, R., Corvalán, J., Flueh, E.R., Hinz, K., Korstgard, J., Ranero, C.R., Weinrebe, W., the CONDOR Scientists, 1997. Tectonic Control of the subducting Juan Fernández Ridge on the Andean margin near Valparaíso, Chile. Tectonics 16 (3), 474–488.